Characterization of Single-Reed Instrument Sound Generation Based on Ffowcs Williams-Hawkings Analogy

Song Wang
song.wang5@mail.mcgill.ca

Esteban Maestre
esteban.maestre@mcgill.ca

Gary Scavone
gary.scavone@mcgill.ca

Computational Acoustic Modeling Laboratory (CAML)
Centre for Interdisciplinary Research in Music Media and Technology (CIRMMT)
Schulich School of Music, McGill University

ABSTRACT

The Ffowcs Williams-Hawkings (FW-H) acoustic analogy is applied to investigate the sound generation of a single-reed instrument. An FW-H formulation is derived using the one-dimensional Green's function for an infinitely long pipe, which estimates the outgoing acoustic pressure at an observer placed inside the instrument via a surface integral of hydrodynamic variables in the mouthpiece-reed system. The FW-H estimation is based on a two-dimensional computational aeroacoustic model developed with the lattice Boltzmann (LB) method, which computes the integrands in the FW-H formulation. The FW-H acoustic analogy is validated by comparing the estimated pressure at the observer to that simulated by the LB model and a good agreement is found. The outgoing pressure at the observer is further decomposed into contributions from monopole and dipole sources, which correspond to different terms in the FW-H formulation. The monopole sources come from the modulated jet flow entering the mouthpiece and the displacement flow induced by the moving reed, whereas dipole sources are produced by the unsteady force exerted on the fluid by the solid walls. Results show that dipole sources, particularly those associated to the long inclined mouthpiece baffle, dominate the observed pressure at the studied playing frequency of 230 Hz.

1. INTRODUCTION

The sound generation of a single-reed instrument is a multiphysics problem that involves acoustics, fluid dynamics and solid vibrations. When a player plays the instrument, the air flows from the lungs toward the instrument, causing the pressure to build up in the player's mouth. The mouth pressure drives the air to flow through the reed aperture at the tip of the mouthpiece into the instrument. In the meantime, the mouth pressure forces the reed to move toward the mouthpiece, and the moving reed in turn modulates the airflow going through the reed channel. The moving reed also creates airflow, and the so-called reed-induced flow disturbs the air in the acoustic resonator together with the pressure-driven flow. The air disturbance travels back and forth in the resonator, and the reflected energy is fed into the mouthpiece-reed system to support the reed oscillation.

The scientific study of single-reed instrument sound generation can be traced back to the 1860s when Helmholtz [1] theoretically investigated the interaction between the reed and the pipe. More recent researchers, such as Backus [2], Benade [3], Nederveen [4], and Worman [5], contributed to the development of a more general mathematical framework for single-reed instrument sound generation. Such a model assumes a localized interaction between the reed, flow, and pipe, which implies that

- the distributed reed vibration is simplified as a single-degree-of-freedom oscillator,
- the distributed airflow and its interaction with the reed is localized at the tip of the reed, and
- the interaction between the resonator and the generator (mouthpiece-reed system) is localized at the entry of the resonator.

This model serves as the basis of sound synthesizers [6] and nonlinear dynamical system studies [7], and it has been widely applied to explore the instrument's sound properties and oscillation.

In addition to this simplified model, the computational fluid dynamics (CFD) and computational aeroacoustic (CAA) models have been applied to investigate the fluid-structure-acoustic interaction in a distributed physical space. These models have shed light on several aspects of sound generation, such as the quasistationary assumption of the fluid model and its dependence on the mouthpiece geometry [8, 9], the effects of the lip on the sound generation [10, 11], and the influences of the mouthpiece geometry on the sound [9, 12]. However, in terms of sound generation, there has been more discussion of aerodynamics than aeroacoustics, and an efficient way to connect the near-field fluid dynamics in the mouthpiece-reed system to the far-field radiated sound characteristics has yet to be established.

This paper aims at a better understanding of the sound generation and a more in-depth characterization of the sound sources of the single-reed instrument. A two-dimensional (2D) computational aeroacoustic model is built for the single-reed instrument using the lattice Boltzmann (LB) method, and the Ffowcs Williams and Hawkings (FW-H) acoustic analogy is employed to estimate the acoustic pressure in the pipe using LB simulation results in the mouthpiece. The FW-H analogy helps decompose the

sound source into distributed monopole and dipole contributions, which are attributed to different sound generation mechanisms and different parts of the mouthpiece-reed system. This work is very much inspired by the research in human phonation [13,14], which made use of the Ffowcs Williams-Hawkings acoustic analogy to characterize the human phonation sound generation mechanisms. A similar analysis routine is used here in studying the same problem but for a single-reed instrument.

2. COMPUTATIONAL AEROACOUSTIC MODELING OF THE SINGLE-REED INSTRUMENT

2.1 Lattice Boltzmann Method

The lattice Boltzmann method (LBM) is an alternative to traditional Navier-Stokes solvers for solving computational fluid dynamics problems. It is based on the lattice Boltzmann equation (LBE), which is obtained by discretizing the mesoscopic-scale Boltzmann equation in physical space, velocity space and time. The LBE is given as

$$f_i(\boldsymbol{x} + \boldsymbol{e}_i\Delta t, t + \Delta t) = f_i(\boldsymbol{x}, t) + \Omega_i(\boldsymbol{x}, t), \quad (1)$$

where f_i is the particle distribution function, e_i is the discrete velocity, Δt is the lattice-unit time step that usually equals 1, and $\Omega(\boldsymbol{x}, t)$ is the collision operator that models the redistribution of the particle population after collisions between particles. The D2Q9 model is used in this paper, which discretizes the velocity space into nine directions for a two-dimensional space. The lattice sound speed is defined as $c_s = 1/\sqrt{3}$, the weight coefficients w_i are set as

$$w_i = \begin{cases} \frac{4}{9}, & i = 0, \\ \frac{1}{9}, & i = 2, 4, 6, 8, \\ \frac{1}{36}, & i = 1, 3, 5, 7, \end{cases} \quad (2)$$

and $\boldsymbol{e}_i$ is given as

$$\boldsymbol{e}_i = \begin{cases} (0, 0), & i = 0, \\ (\cos\frac{(i+2)\pi}{4}, \sin\frac{(i+2)\pi}{4}), & i = 2, 4, 6, 8, \\ \sqrt{2}(\cos\frac{(i+2)\pi}{4}, \sin\frac{(i+2)\pi}{4}), & i = 1, 3, 5, 7. \end{cases} \quad (3)$$

The collision is modeled with recursive regularized BGK (rrBGK) [15], which is known to provide greater numerical accuracy and a more stable simulation for high Mach number and high Reynolds number flow by filtering out non-hydrodynamic components in the solution.

Palabos [16], an open-source LBM-based computational fluid dynamics framework, is used for the numerical simulation.

2.2 Mouthpiece Model

The schematic of the simulation setup is shown in Figure 1. The pressure source is placed at the inlet of the computational domain using the absorbing boundary condition (ABC) proposed by Kam et al. [17]. The immersed boundary method (IBM) [18] is used to model the walls of the mouthpiece and reed, as well as their interaction

with the surrounding fluid. The IBM is only applied to the complex geometry of the mouthpiece before the throat (the junction between the chamber and the cylindrical parts of the mouthpiece), whereas the Zou-He boundary condition [19] is applied to the rest of the solid walls, including the walls in the cylindrical bore and mouth cavity. The immersed boundary (IB) nodes and Zou-He boundaries are represented by dotted and solid lines in Figure 1, respectively.

The mouthpiece geometry was derived from a CT (computed tomography) scan of a Meyer® 5M alto saxophone mouthpiece with a tip opening of 1.8 mm. The length of the cylindrical part of the mouthpiece, known as the mouthpiece bore, is 1 cm with a diameter of 1.5 cm. A 2D pipe with the same diameter and a length of 30 cm is attached to the mouthpiece. The characteristic-based time-domain impedance boundary condition (C-TDIBC) [20] is applied to the end of the pipe, where an unflanged cylindrical pipe radiation impedance Z_{rad} is employed to represent the radiation domain. The applied radiation impedance is derived from a s-domain polynomial approximation of the radiation coefficients [21], which is transformed to the z-domain using the bilinear transform.

The sound speed is set to $343\,\text{m/s}$. The kinetic viscosity is set to $1.51e^{-4}\,\text{m}^2/\text{s}$, which is an order of magnitude larger than that of the air to guarantee a stable simulation. The grid size and time step are $\Delta x \approx 9.53e^{-5}$ m and $\Delta t \approx 1.60e^{-7}$ s, correspondingly, which guarantees a 360 point-per-wavelength at $10\,\text{kHz}$.

2.3 Reed Model

The one-dimensional (1D) distributed reed model proposed by Avanzini et al. [22] is used in the present study, and the mouthpiece-reed-lip interaction is illustrated in Figure 2. The reed is modeled in a separate coordinate $(x_{\text{reed}}, y_{\text{reed}})$ in the LB domain, as illustrated in Figure 1, and the subscripts are omitted for simplicity in this section.

The reed is modeled as a clamped bar with its transverse oscillation amplitude y governed by the following Euler-Bernoulli equation:

$$\frac{\partial^2}{\partial x^2}\left[YI(x)\left(1 + \eta\frac{\partial}{\partial t}\right)\frac{\partial^2 y}{\partial x^2} \right] + \rho_r S(x)\left[\frac{\partial^2 y}{\partial t^2} + \gamma_B\frac{\partial y}{\partial t}\right] = F(x, t), \quad (4)$$

where ρ_r is the reed density, Y is the Young's modulus, and η is the magnitude of the internal viscoelastic losses. $I(x) = S(x)\kappa^2(x)$ represents the moment of inertia about the longitudinal axis with $\kappa(x)$ representing the radius of gyration of the cross-section $S(x) = wb(x)$, where w and $b(x)$ represent the width and thickness of the reed.

The force applied on the reed $F(x, t) = F_{\text{lay}}(x, t) + F_{\text{lip}}(x, t) + F_{\text{fluid}}(x, t)$ is composed of the contact force due to the collision between the reed and the lay, the lip force distributed over a contact area of the reed with the lip, and the aerodynamic force from the surrounding fluid.

The contact force F_{lay} comprises the elastic force F_{el} and dissipative force F_{dis}, which are defined correspondingly
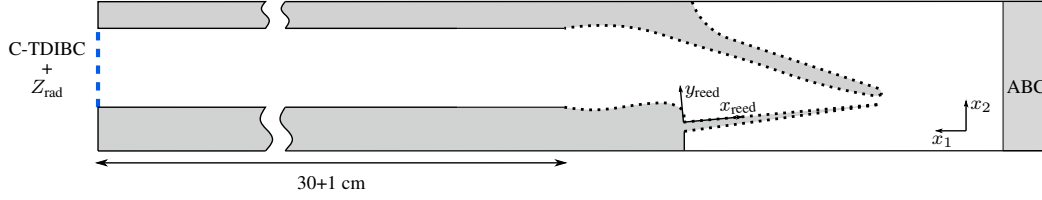
Figure 1. The schematic view of the computational domain.

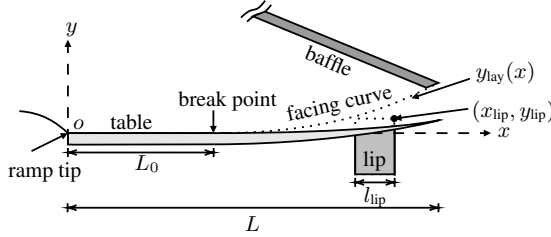
Figure 2. The schematic view of the mouthpiece-reed-lip interaction.

as

$$F_{\text{dis}}(x,t) = \rho_r S(x)\dot{y}(x,t)/\Delta t, \qquad (5)$$

and

$$F_{\text{el}}(x,t) = \begin{cases} -K_{\text{lay}}\Delta y_{\text{lay}}(x,t) & \Delta y_{\text{lay}} > 0, \\ 0 & \text{otherwise}, \end{cases} \qquad (6)$$

where $\Delta y_{\text{lay}}(x,t) = y(x,t) - y_{\text{lay}}(x)$, and the profile of the lay is fit by a fourth-order polynomial, as

$$y_{\text{lay}}(x) = \begin{cases} \sum_{n=0}^{4} l_n(x - L_0)^n, & x > L_0, \\ 0, & x <= L_0. \end{cases} \qquad (7)$$

The lip provides both elastic and damping forces, where $F_{\text{lip}} = -k_{\text{lip}}\Delta y_{\text{lip}}$, with $\Delta y_{\text{lip}} = y_{\text{lip}} - y(x,t) + b(x)$ representing the compression of the lip. The damping effect is included by modifying the damping coefficient γ_B, where

$$\gamma_B = \begin{cases} \gamma_{\text{air}} + \gamma_{\text{lip}}, & x \in (x_{\text{lip}} - L_{\text{lip}}, x_{\text{lip}}), \\ \gamma_{\text{air}} & \text{otherwise}. \end{cases} \qquad (8)$$

The time discretization of Equation (4) is consistent with that of the LB simulation. The spatial discretization relies on the discretized immersed boundary nodes of the reed. The distance between nodes is set to $0.45\Delta x$, where Δx is the LB grid size. The IB nodes located at the top of the reed are evenly distributed along the y-axis, and the bottom IB reed nodes are placed based on the thickness function $b(x)$. The reed model has an equal number of IB nodes on the top and bottom, and the F_{fluid} is calculated by subtracting the IB force exerted on the top reed nodes from corresponding ones on the bottom. The IBM is used to update the IB force in the LB simulation at each time step.

3. FFOWCS WILLIAMS-HAWKINGS ACOUSTIC ANALOGY

The acoustic analogy was proposed by Lighthill who reformulated the Navier-Stokes equation into an inhomogeneous wave equation [23]. The nonlinear terms are moved to the righthand side (RHS) of the equation and are considered as the sound source. Ffowcs Williams and Hawkings extended Lighthill's acoustic analogy by introducing moving boundaries [24], resulting in the FW-H equation, written as

$$\left(\frac{1}{c_\infty^2}\frac{\partial^2}{\partial t^2} - \frac{\partial^2}{\partial x_i^2}\right)[\rho' c_\infty^2 H] = \frac{\partial^2(HT_{ij})}{\partial x_i \partial x_j} + \frac{\partial F_i}{\partial x_i} + \frac{\partial Q}{\partial t}, \qquad (9)$$

where H is the Heaviside function, c_∞ is the speed of the sound in the quiescent flow and

$$T_{ij} = \rho v_i v_j + [p' - \rho' c_\infty^2]\delta_{ij} - \tau_{ij},$$

$$F_i = -(\rho v_i(v_j - \bar{v}_j) + p_{ij})\frac{\partial H}{\partial x_j},$$

$$Q = (\rho v_j - \rho' \bar{v}_j)\frac{\partial H}{\partial x_j},$$

and τ_{ij} is the viscous shear stress, v_j and $\bar{v}_j$ represent the velocities of the flow and solid wall, respectively.

The three source terms on the RHS correspond, respectively, to

- the *quadrupole* sound source $\partial^2(HT_{ij})/\partial x_i \partial x_j$ due to the distributed Lighthill stress tensor T_{ij} in the volume,
- the *dipole* sound source $\partial F_i/\partial x_i$ generated by
  - the compressive stress p_{ij} applied to the fluid by the surface, and
  - the momentum flux $\rho v_i(v_j - \bar{v}_j)$ through the surface, and
- the *monopole* sound source $\partial Q/\partial t$ contributed by the mass flux $\rho v_j - \rho' \bar{v}_j$ across the surface.

The solution to the FW-H equation is obtained by convolving the sound source, i.e. the RHS of Equation (9), with the Green's function $G(\boldsymbol{x}, t|\boldsymbol{y}, \tau)$, and the result is stated in the following form after a series of simplifications [25]:

$$\rho'(\boldsymbol{x},t)c_\infty^2 = \int_{-\infty}^{t}\int_V \frac{\partial^2 G}{\partial y_i \partial y_j}T_{ij}\mathrm{d}V(\boldsymbol{y})\mathrm{d}\tau$$
$$+ \int_{-\infty}^{t}\int_S \frac{\partial G}{\partial y_i}[\rho v_i(v_j - \bar{v}_j) + p_{ij}]\,n_j\mathrm{d}S(\boldsymbol{y})\mathrm{d}\tau$$
$$- \int_{-\infty}^{t}\int_S \frac{\partial G}{\partial \tau}[(\rho v_j - \rho' \bar{v}_j)n_j]\,\mathrm{d}S(\boldsymbol{y})\mathrm{d}\tau. \qquad (10)$$

The integral surface S and integral volume V for the FW-H formulation in a single-reed instrument are illustrated in Figure 3. The integral surface is composed of the inlet S_{in},
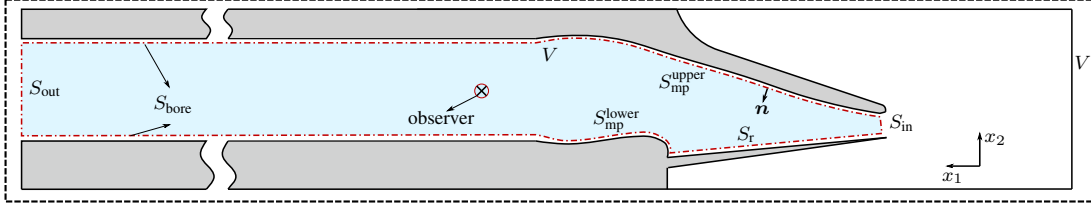
Figure 3. The integral surface of FW-H acoustic analogy with the normals of the surface $\boldsymbol{n}$ pointing into the fluid.

outlet S_{out}, and solid walls $S_w = S_{\text{mp}}^{\text{upper}} + S_{\text{mp}}^{\text{lower}} + S_r + S_{\text{bore}}$ that include the upper $S_{\text{mp}}^{\text{upper}}$ and lower $S_{\text{mp}}^{\text{lower}}$ parts of the mouthpiece, the bore S_{bore}, as well as the reed top surface S_r. The normal $\boldsymbol{n}$ of the integral surface is pointing into the mouthpiece. The integral volume includes only the area inside the instrument and excludes the mouth cavity and radiation domain. In addition, the area in the reed channel (the space between the mouthpiece tip rail and the reed) is not included in the integral volume, and the inlet S_{in} is placed at the end of the mouthpiece reed channel. This is made to eliminate the potential for an unclear definition of the integral surface in the reed channel during the beating of the reed with the mouthpiece.

In the present study, the observer is placed 8 mm away from the mouthpiece throat in the cylindrical bore. It is worth mentioning that in contrast to external flow applications, the observer in single-reed instruments cannot be placed in an acoustic far field due to the presence of standing waves inside the instrument. Therefore, the observer has to be placed in the acoustic near field, which is one of the primary differences between the present FW-H application in single-reed instruments and previous research in human phonation, where the vocal tract was replaced with an infinite pipe without acoustic feedback.

The one-dimensional Green's function for an infinite pipe is used to solve the FW-H equation

$$G(x_1, t | y_1, \tau) = \frac{c_\infty}{2S} H(t - \tau - |x_1 - y_1|/c), \quad (11)$$

where S is the cross-section area at the observer.

Based on the integral domain specified in Figure 3, the FW-H formulation is shown as follows:

$$
\begin{aligned}
\rho'(x_1, t) c_\infty^2 = {} & \frac{1}{2c_\infty S} \frac{\partial}{\partial t} \int_V [T_{11}]_{t^*} \, \mathrm{d}V(\boldsymbol{y}) \\
& + \frac{1}{2S} \int_{S_w} [p_{1j} n_j]_{t^*} \, \mathrm{d}S(\boldsymbol{y}) \\
& + \frac{c_\infty}{2S} \int_{S_r} [\rho_\infty \bar{v}_j n_j]_{t^*} \, \mathrm{d}S(\boldsymbol{y}) \\
& + \frac{1}{2S} \int_{S_{\text{in}}} [(\rho v_1 v_1 + p_{11}) + \rho c_\infty v_1]_{t^*} \, \mathrm{d}S(\boldsymbol{y}) \\
& + \frac{1}{2S} \int_{S_{\text{out}}} [(\rho v_1 v_1 + p_{11}) - \rho c_\infty v_1]_{t^*} \, \mathrm{d}S(\boldsymbol{y}),
\end{aligned}
$$
$$(12)$$

where $t^* = t - |x - y|/c$ is the retarded time.

In this formulation, the first term corresponds to the quadrupole sound source, which arises due to the Lighthill stress tensor in the control volume. The second term represents the dipole sound source contributed by the force exerted on the fluid by the solid walls, while the third term accounts for the monopole sound source produced by the induced displacement flow of the moving reed. Theoretically, the fourth and fifth terms are combinations of the dipole contribution by $\rho v_1 v_1 + p_{11}$ and the monopole contribution by ρv_1. However, these terms can also be treated as equivalent monopoles produced by the mass flux across the inlet and outlet surfaces $\rho v_1 M_1 + \rho v_1^{\pm}$, where $M_1 = v_1/c_\infty$ is the Mach number in x_1-direction, and $v_1^{\pm} = p_{11}/\rho c \pm v_1$ represents the incoming acoustic velocities. It should be noted that both S_{out} and S_{in} are defined perpendicular to the x_1-axis, so that their normal vectors n_j are correspondingly replaced with $(-1, 0)$ and $(1, 0)$ during the derivation.

The above formulation can be further simplified by omitting the quadrupole term, since its magnitude is typically two orders lower than that of the dipole [13]. Additionally, the dipole contribution from the bore S_{bore} is zero, owing to the wall's parallel orientation with respect to the x_1-axis. Consequently, the second to fourth sound source terms are all located upstream of the observer so that they only contribute to the left-going pressure $p^+(x_1, t)$ at the observer's position. On the other hand, the fifth term represents the only sound source located downstream of the observer and contributes exclusively to the right-going pressure $p^-(x_1, t)$.

Given that the present study focuses on sound generation within the mouthpiece, the final FW-H formulation, which evaluates the left-going pressure at the observer using only upstream surface integral, is as follows:

$$
\begin{aligned}
p^+(x_1, t) = {} & \frac{1}{2S} \int_{S_{w'}} [p_{1j} n_j]_{t^*} \, \mathrm{d}S(\boldsymbol{y}) \\
& + \frac{c_\infty}{2S} \int_{S_r} [\rho_\infty \bar{v}_j n_j]_{t^*} \, \mathrm{d}S(\boldsymbol{y}) \\
& + \frac{1}{2S} \int_{S_{\text{in}}} [(\rho v_1 v_1 + p_{11}) + \rho c_\infty v_1]_{t^*} \, \mathrm{d}S(\boldsymbol{y}),
\end{aligned}
$$
$$(13)$$

where the total wall surface area is defined as $S_{w'} = S_{\text{mp}}^{\text{upper}} + S_{\text{mp}}^{\text{lower}} + S_r$. The three different terms are referred to as the dipole, reed monopole, and inlet monopole, respectively, in later discussions.

4. RESULTS AND DISCUSSION

The reed and lip parameters are set so that the instrument can play near its first resonant frequency. The mouth pressure increases from 0 to 6000 Pa in 5 ms and remains steady for 45 ms until the end of the simulation.

The LB simulated outgoing pressure at the observer is calculated as $(\tilde{p}+\rho c\tilde{v})/2$, where $\tilde{p}$ and $\tilde{v}$ represent spatially averaged pressure and velocity over the cross-section area at the observer, respectively. Equation (13) is used to compute the FW-H estimation, with the integrands calculated using the LB simulated values on the integral surface.

Figure 4 displays the time-domain comparison between the LB simulated pressure and the FW-H estimation, which shows a good agreement in both the transient and steady-state signals. The spectra of the steady-state signal are calculated using the "period synchronized sampling" technique [26], and are compared in Figure 5. It also shows a good overall agreement with the largest deviation less than 3 dB.
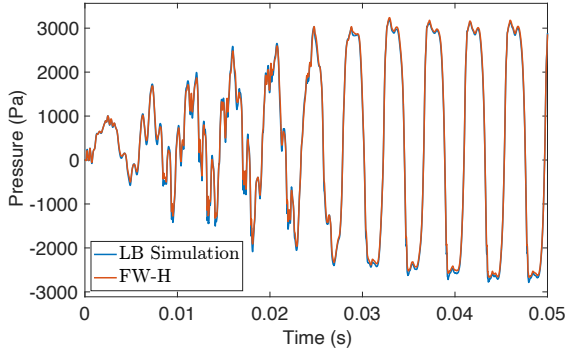

Figure 4. The time-domain comparison between the LB simulated outgoing pressure at the observer and the estimated one using the FW-H formulation.

One of the main benefits of using the FW-H acoustic analogy is its ability to decompose the sound into contributions from various sound generation mechanisms. The equivalent sound level L_{eq} is used to measure the strength of different sound sources:

$$L_{\mathrm{eq}} = 10\log\frac{1}{T}\int\frac{p(t)^2}{p_0^2}\mathrm{d}t, \qquad (14)$$

where p is the sound pressure signal, $p_0 = 20\,\mu\mathrm{Pa}$ is the reference pressure, and T is the period of the signal.

The sound sources are decomposed into the dipole, reed monopole, and inlet monopole, corresponding to the first to third terms in Equation (13), respectively. Their time-domain signals are compared in Figure 6, and the L_{eq} of steady-state signals are 181.2 dB, 153.9 dB, and 164.8 dB, correspondingly. It is clear that the dipole sources, which are generated by the unsteady-force exerted by the solid walls to the fluid, contribute the most to the outgoing pressure at the observer. This seems paradoxical because one may assume the modulated jet flow through the reed channel to be the main source in single-reed instrument sound generation. Such a contrary finding mainly comes from the fact that the fluctuating force that contributes to the dipole in FW-H with the 1D Green's function for an infinite pipe is not only composed of the fluctuation in rotational fluid fields such as the vortices, but also the acoustic fluctuation, which is essentially the acoustic response of the mouthpiece solid walls' to the incoming wave from the

resonator. In other words, the dipole contributed by the $\frac{1}{2S}\int_{S_{w'}}[p_{1j}n_j]_{t*}\mathrm{d}S(\boldsymbol{y})$ not only accounts for the sound source due to the presence of solid walls in the fluid, but also for the interaction of reflected sound from the resonator with the solid walls [27], which is related to the role of the mouthpiece as an acoustic resonator [28]. The dipole-dominant feature can also be attributed to the choice of the Green's function. If a one-dimensional Green's function for a semi-infinite pipe terminated at the inlet is chosen, a quadrupole source will emerge from the dipole sources and their image dipoles placed on the other side of the closed end. Because quadrupoles are known to be radiationally inefficient, they might contribute less than the monopole sources. In addition, a new monopole sound source will arise from the outlet, which generates an image monopole that represents the reflection of the incoming acoustic wave by the closed end.

Because a closed reed channel cancels the S_{in}, and therefore the inlet's contribution to the sound at the observer, the inlet monopole contributes almost exclusively to the positive pressure signal. The waveform of the reed monopole is similar to that of the inlet monopole because they are both dependent on reed displacement. The reed monopole contribution, on the other hand, is delayed, which is mainly attributed to the 90-degree lag in phase between the reed velocity and reed displacement, which are correspondingly reflected in the monopole terms of the reed and inlet. Furthermore, the amplitude of the reed monopole is about 10 dB lower than that of the inlet monopole. However, the relative strength of the reed monopole to the inlet monopole should be frequency-dependent. Further investigation is necessary to fully assess their relationship.

The dipole sound source is further decomposed into contributions by different walls, and the upper mouthpiece is discovered to be the strongest dipole, as indicated in Figure 7. This is primarily attributed to the long inclined baffle connecting the end of the reed channel to the mouthpiece throat. The dipole contributions from the reed and lower mouthpiece are comparable in amplitude but out of phase, whereas the reed dipole is roughly in phase with the upper mouthpiece dipole. This is because the upper mouthpiece and reed are oriented in the positive direction of x_1, while the ramped wall of the lower mouthpiece is facing in the opposite direction, resulting in a different sign of the axial normal vectors n_1 when computing the dipole contribution, and hence a $180°$ phase difference. The distribution on solid walls of the compressive stress $(p_{1j}n_j)$ root-mean-square values is presented in Figure 8, which helps better illustrate the natures of different dipole contributions.

5. CONCLUSIONS

A 2D computational aeroacoustic model was built using the lattice Boltzmann method to investigate the single-reed instrument sound generation. The Ffowcs Williams and Hawkings acoustic analogy is employed to analyze the sound generation mechanisms. It helps decompose the outgoing pressure at the observer in the pipe into contributions by different monopoles and dipoles distributed in the
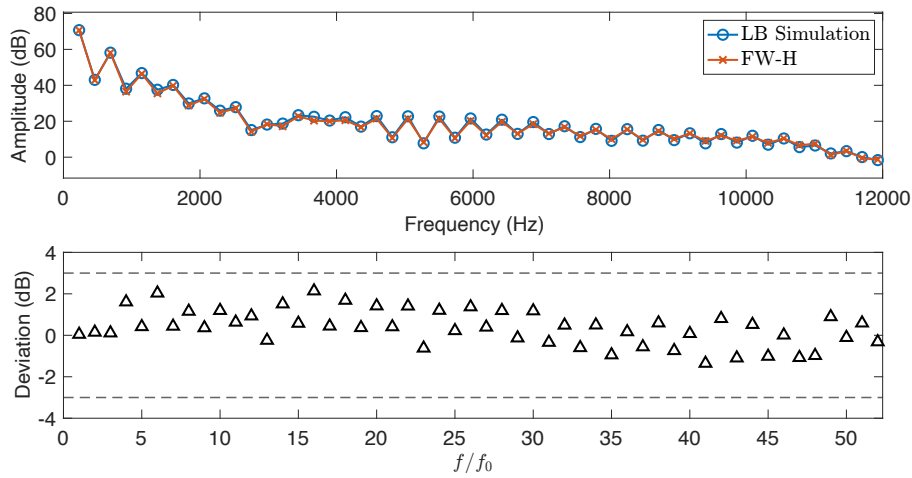
Figure 5. The comparison of the outgoing pressure spectra between the LB simulation and FW-H estimation (top), and the amplitude deviations in dB of harmonics below 12 kHz (bottom).
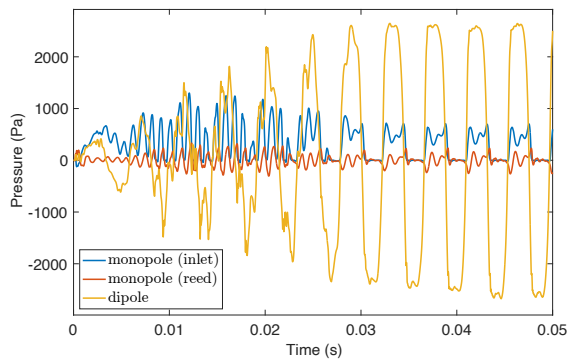

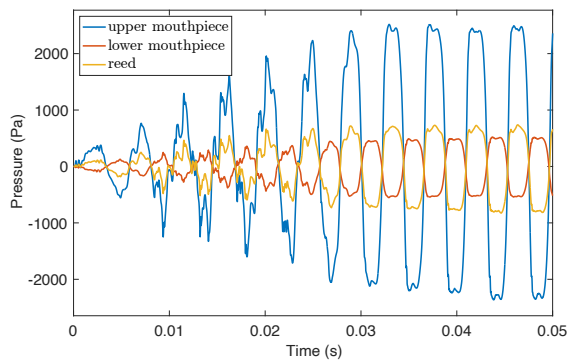Figure 6. The comparison between different contributions to the outgoing pressure at the observer.

Figure 7. The comparison of dipole sound sources contributed by different solid walls.

Figure 8. (a) The distribution of $(p_{1j}n_j)_{\mathrm{rms}}$ along the solid walls, and (b) the mouthpiece geometry.

mouthpiece-reed system. The LB simulation results are used to calculate the strength of different sound sources, and the dipole sources, especially the one distributed along the mouthpiece baffle, are the dominant sound sources at the playing frequency considered (around 230 Hz). The FW-H acoustic analogy has been shown to be an effective
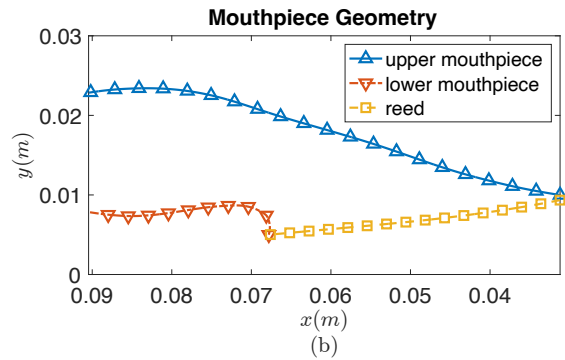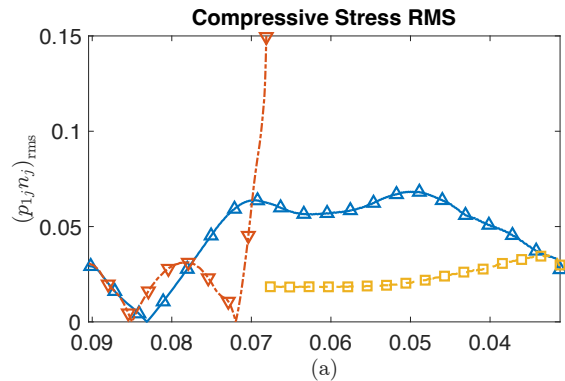
technique for studying the sound generation of the single-reed instrument. It not only provides additional insights of the sound generation characteristics of the instrument, but also builds a direct correlation between the mouthpiece geometry and the sound, which is useful in mouthpiece design.

The main limitation of the present study is the 2D nature of the computational aeroacoustic model, which lacks

the ability to reproduce some of the phenomena found in a real single-reed instrument, such as turbulence and the side slits of the mouthpiece-reed system. However, the present study can be easily extended to a 3D computational aeroacoustic model and use the same FW-H formulation to characterize the sound generation. It is worthwhile to compare the results of a 3D model with those found in this paper, particularly inlet monopole contributions, which are expected to be larger in a 3D model due to the contribution from side slits.

In addition, the dipole-dominant characteristic is partially due to the choice of Green's function. It would be beneficial to derive a FW-H formulation using the low frequency Green's function for a 1D semi-infinitely long pipe terminated at the inlet. This will allow for comparison with the findings presented in this paper, thereby providing further insights into single-reed instrument sound generation mechanisms.

More simulations at different playing frequencies can be studied in the future to characterize the frequency-dependency of different sound sources. Furthermore, it may be interesting to investigate how much the fluid field inside the mouthpiece influences the dipole strength by comparing the present aeroacoustic model with a linear acoustic mouthpiece model, such as the transfer matrix mouthpiece model [28] or transmission line mouthpiece model [29].

Acknowledgments

6. REFERENCES

[1] H. Helmholtz, *On the Sensations of Tone as a Physiological Basis for the Theory of Music*, 2nd ed. New York: Peter Smith, 1885.

[2] J. Backus, "Small-vibration theory of the clarinet," *The Journal of the Acoustical Society of America*, vol. 35, no. 3, pp. 305–313, 1963.

[3] A. H. Benade and D. J. Gans, "Sound production in wind instruments," *Annals of the New York Academy of Sciences*, vol. 155, no. 1, pp. 247–263, 1968.

[4] C. J. Nederveen, *Acoustical Aspects of Woodwind Instruments*. Northern Illinois University Press, 1969.

[5] W. E. Worman, "Self-Sustained Nonlinear Oscillations of Medium Amplitude in Clarinet-Like Systems." Ph.D. dissertation, Case Western Reserve University, 1971.

[6] P. Guillemain, "A digital synthesis model of double-reed wind instruments," *EURASIP Journal on Applied Signal Processing*, vol. 2004, pp. 990–1000, 2004.

[7] S. Karkar, "Méthodes numériques pour les systèmes dynamiques non linéaires: Application aux instruments de musique auto-oscillants," Ph.D. dissertation, Aix-Marseille, 2012.

[8] A. R. da Silva, G. P. Scavone, and M. van Walstijn, "Numerical simulations of fluid-structure interactions in single-reed mouthpieces," *The Journal of the Acoustical Society of America*, vol. 122, no. 3, pp. 1798–1809, Sep. 2007.

[9] Y. Shi, "A numerical framework for fluid-acoustic-structure interaction in clarinet-like instruments," Ph.D. dissertation, McGill University, 2016.

[10] N. Giordano and J. W. Thacker, "Navier-Stokes-based model of the clarinet," *The Journal of the Acoustical Society of America*, vol. 148, no. 6, pp. 3827–3835, Dec. 2020.

[11] T. Yoshinaga, H. Yokoyama, T. Shoji, A. Miki, and A. Iida, "Numerical investigation of effects of lip stiffness on reed oscillation in a single-reed instrument," *The Journal of the Acoustical Society of America*, vol. 149, no. 4, pp. A68–A68, Apr. 2021.

[12] ——, "Numerical investigation of effects of mouthpiece geometry on flow and sound generation in a single-reed instrument," in *Proceedings of the 24th International Congress on Acoustics*, Gyeongju, Korea, 2022 Oct.

[13] W. Zhao, C. Zhang, S. H. Frankel, and L. Mongeau, "Computational aeroacoustics of phonation, Part I: Computational methods and sound generation mechanisms," *The Journal of the Acoustical Society of America*, vol. 112, no. 5, pp. 2134–2146, 2002.

[14] C. Zhang, W. Zhao, S. H. Frankel, and L. Mongeau, "Computational aeroacoustics of phonation, Part II: Effects of flow parameters and ventricular folds," *The Journal of the Acoustical Society of America*, vol. 112, no. 5, pp. 2147–2154, 2002.

[15] O. Malaspinas, "Increasing stability and accuracy of the lattice Boltzmann scheme: Recursivity and regularization," *arXiv preprint arXiv:1505.06900*, 2015.

[16] J. Latt, O. Malaspinas, D. Kontaxakis, A. Parmigiani, D. Lagrava, F. Brogi, M. B. Belgacem, Y. Thorimbert, S. Leclaire, and S. Li, "Palabos: Parallel lattice Boltzmann solver," *Computers & Mathematics with Applications*, vol. 81, pp. 334–350, 2021.

[17] E. W. S. Kam, R. M. C. So, and R. C. K. Leung, "Lattice Boltzmann method simulation of aeroacoustics and nonreflecting boundary conditions," *AIAA journal*, vol. 45, no. 7, p. 1703, 2007.

[18] T. Inamuro, "Lattice Boltzmann methods for moving boundary flows," *Fluid Dynamics Research*, vol. 44, no. 2, p. 024001, 2012.

[19] Q. Zou and X. He, "On pressure and velocity boundary conditions for the lattice Boltzmann BGK model," *Physics of fluids*, vol. 9, no. 6, pp. 1591–1598, 1997.

[20] S. Wang, E. Maestre, and G. Scavone, "Lattice Boltzmann Modeling of a Single-Reed Instrument Using a Time-Domain Impedance Boundary Condition," in *Fourth Vienna Talk on Music Acoustics*, Vienna, Austria, 2022.

[21] F. Silva, P. Guillemain, J. Kergomard, B. Mallaroni, and A. N. Norris, "Approximation formulae for the acoustic radiation impedance of a cylindrical pipe," *Journal of Sound and Vibration*, vol. 322, no. 1, pp. 255–263, 2009.

[22] F. Avanzini and M. Van Walstijn, "Modelling the mechanical response of the reed-mouthpiece-lip system of a clarinet. Part I. A one-dimensional distributed model," *Acta Acustica united with Acustica*, vol. 90, no. 3, pp. 537–547, 2004.

[23] M. J. Lighthill, "On sound generated aerodynamically I. General theory," *Proceedings of the Royal Society of London A: Mathematical, Physical and Engineering Sciences*, vol. 211, no. 1107, pp. 564–587, Mar. 1952.

[24] J. E. Ffowcs Williams and D. L. Hawkings, "Sound generation by turbulence and surfaces in arbitrary motion," *Philosophical Transactions of the Royal Society of London A*, vol. 264, no. 1151, pp. 321–342, 1969.

[25] S. Glegg and W. Devenport, *Aeroacoustics of Low Mach Number Flows: Fundamentals, Analysis, and Measurement*. Academic Press, 2017.

[26] T. Grothe, "Experimental Investigations of Bassoon Acoustics," Ph.D. dissertation, Technische Universität Dresden, 2013.

[27] M. S. Howe, *Theory of Vortex Sound*, ser. Cambridge Texts in Applied Mathematics. Cambridge University Press, 2003.

[28] S. Wang, E. Maestre, and G. Scavone, "Acoustical modeling of the saxophone mouthpiece as a transfer matrix," *The Journal of the Acoustical Society of America*, vol. 149, no. 3, pp. 1901–1912, Mar. 2021.

[29] S. Wang, G. Scavone, and E. Maestre, "Two methods for acoustic modeling of the saxophone mouthpiece," *The Journal of the Acoustical Society of America*, vol. 148, no. 4, pp. 2611–2611, Oct. 2020.